www.ietdl.org

Published in IET Communications
Received on 30th April 2014
Revised on 29th July 2014
Accepted on 10th September 2014
doi: 10.1049/iet-com.2014.0432

ISSN 1751-8628

Indoor free space optics link under the weak turbulence regime: measurements and model validation

Riccardo Pernice[1], Andrea Andò[1], Marzia Cardinale[1], Luciano Curcio[1], Salvatore Stivala[1], Antonino Parisi[1], Alessandro C. Busacca[1], Z. Ghassemlooy[2], Joaquin Perez[3]

[1]*Department of Energy, Information Engineering and Mathematical Models (DEIM), University of Palermo, Viale delle Scienze Bld. 9 – 90128 Palermo, Italy*
[2]*Optical Communications Research Group, NCRLab, Faculty of Engineering and Environment, Northumbria University, Newcastle upon Tyne, NE1 8ST, United Kingdom*
[3]*Optical and Quantum Communications Group, Institute of Telecommunications and Multimedia Applications (iTEAM), Universitat Politècnica de València, 46022, València, Spain*
E-mail: riccardo.pernice@unipa.it

Abstract: In this study, the authors present the measurements performed on a free space optics (FSO) communications link using an indoor atmospheric chamber. In particular, the authors have generated several different optical turbulence conditions, demonstrating how even the weak turbulence regime can strongly affect the FSO link performance. The authors have carried out an in-depth analysis of the data collected during the measurements, and calculated the turbulence strength (i.e. scintillation index and Rytov variance) and the important performance metrics (i.e. the Q-factor and bit error rate) to evaluate the FSO link quality. Moreover, the authors have tested, for the first time, an appositely developed temporally-correlated gamma–gamma channel model to generate the temporal irradiance fluctuations observed at the receiver. This has been accomplished by using a complete analysis tool that enables the authors to fully simulate the experimental FSO link. Finally, the authors compare the generated time-series with the collected experimental data, showing a good agreement and thus proving the effectiveness of the model.

1 Introduction

Until now, radio frequency (RF) and fibre optics technologies have been largely deployed in urban areas to ensure error-free and high data-rate communications. However, these technologies do not represent the most cost-effective way of providing high-quality video and audio streaming services to the end users. In fact, free space optics (FSO) is a broadband based wireless communication technology offering almost similar capabilities to those of optical fibre communications and several advantages compared with RF links. In particular, FSO links offer higher transmission rates over a wide unlicensed spectral range of 0.7–10 μm, inherent security, ease of installation and relocation and is a green technology by the way of lower power consumption. Moreover, FSO systems do not interfere with other wireless communications links [1]. With such features, the FSO technology is attractive for range of applications, including the last mile wireless access network, fibre backup, wireless base station-to-base station, disaster recovery, network extension, building-to-building connectivity and temporary link. It is also widely used to bring high-speed connectivity to rural areas or developing countries, where the deployment of fibre and satellite infrastructures is not affordable, because of their high cost or the low population density [2]. Moreover, FSO systems are also employed in inter-satellite communications and in satellite uplinks/downlinks [3, 4].

The transmitter side of an FSO system usually consists of a laser diode, a modulator (that can either be external or included in the laser driver, in the case of direct modulation) and an optical collimator. The emitted optical signal propagates along the free space channel (i.e. air) and it is collected at the receiver by means of telescope, detector and demodulator. The most common wavelengths used in FSO links are in the range of 0.85–1.55 μm, and more specifically at wavelengths of 780 nm, 850 nm and 1550 nm, with the latter two coinciding with the optical fibre communications first and third transmission windows [1, 5].

Although propagating through the atmosphere, the modulated optical beam can be strongly affected by unfavourable atmospheric conditions, such as clouds, fog, rain, snow, smog – that generate optical scattering – and, furthermore, absorption and scintillation phenomena [6–10]. Moreover, the scintillation is one of the most important factors that, even under the clear sky conditions, can degrade the performance of an FSO communication link. This random phenomenon originates from refractive index fluctuations (i.e. optical turbulence) caused almost exclusively by small temperature

variations in the atmosphere [11, 12]. The atmospheric turbulence produces irradiance fluctuations of the beam, which can cause the optical power to drop below the receiver threshold. In this case, a large number of problems can occur during the communication between the transmitter and the receiver, such as fading and losses. In order to reduce these impairments, several techniques have been reported in the literature. Among hardware solutions, aperture averaging [13, 14] and spatial diversity – such as multiple-input multiple-output (MIMO) based FSO systems [15, 16] – are mostly employed to improve the link performance under different atmospheric turbulence regimes.

Instead, software solutions mainly consist of a retransmission protocol or suitable encoding techniques, such as the recently developed rateless codes [17–19].

To predict the impact of optical turbulence on FSO communications, several turbulence models have been developed and reported in the literature [1, 11, 12] to analyse and describe the irradiance fluctuations at the receiver. Among them, is the log-normal distribution, which is mainly used for the weak turbulence regime, while gamma–gamma (G–G) model can be adopted for all turbulence regimes. Whereas the negative exponential model is mainly employed for very strong turbulence conditions (i.e. the saturation regime). Therefore the G–G model is the most widely used in order to estimate the performance of FSO links under different atmospheric turbulence conditions [20–24].

However, with the above-mentioned models, it is only possible to find out about the irradiance statistics at the receiver. In order to test both software and hardware solutions for fading mitigation, by means of a theoretical or simulative approach, detailed information about the signal fading including the temporal duration and its statistics is needed. In the literature, such information is mainly obtained from the measurements, thus limiting the analysis for given experimental conditions [25, 26]. To overcome this limit, in one of our previous works [27], a high-resolution time-correlated G–G channel model able to predict, at the desired conditions, the random irradiance temporal fluctuations caused by the optical turbulence was presented. In this paper we analyse and test the effectiveness of the above-mentioned model under the weak turbulence conditions for the first time. In details, a comparison between the experimental data collected during a measurement campaign and the simulated data produced by our time-correlated G–G channel model for the given experimental conditions is reported. Moreover, an experimental set-up is presented, where a range of turbulent conditions can be created inside an indoor atmospheric chamber to evaluate the FSO link performance. The in-depth data post-processing has been carried out on the captured data regarding scintillation index and the normalised probability density function (PDF) based on the widely used G–G model. The evaluation of the obtained results will provide a complete comparison with the theoretically predicted distributions. In summary, a complete analysis tool to perform a precise simulation of the experimental FSO link has been implemented in order to compare between the time-series generated by our proposed model and the experimental data.

The rest of the paper is organised as follows: the measurement set-up is introduced and explained in Section 2. The data post-processing procedure implemented to analyse the FSO link performance and the theoretical model of turbulence are outlined in Section 3, whereas the experimental results are discussed in Section 4. The analysis tool able to simulate the experimental FSO links and to compare the time-series generated by using the proposed time-correlated channel model with the collected experimental data is illustrated in Section 5. Conclusions and future works are presented in the final section.

2 Experimental set-up

The measurement campaign was aimed at investigating the performance of the FSO communications link under the influence of the weak atmospheric turbulence regime. The experimental set-up, depicted in Fig. 1, consisted of a dedicated indoor atmospheric chamber [28] having a dimension of $5.5 \times 0.3 \times 0.3$ m^3.

The chamber is composed of seven compartments (not shown in Fig. 1), with each section having a vent for the air circulation. In order to create thermal gradients and hence turbulence, two external fan heaters were used to blow hot air in the direction perpendicular to the propagating optical beam along the chamber through the two open vents placed closer to the transmitter (FHT) and the receiver (FHR) and the rest were kept closed, as depicted in Fig. 1. In this way, the temperature inside the chamber was able to reach up to 50–60°C with a temperature gradient greater than 6°C, along the chamber between the transmitter and receiver, as required for creation of turbulence [1]. In order to continuously monitor the temperature profile along the chamber, three temperature sensors (T1, T2 and T3) at 2.4 m apart were used, see Fig. 1.

On the transmitter side (Tx), a non-return to zero on-off-keying (NRZ-OOK) modulation format at a range of data rates (1, 5 or 10 Mbps) was loaded into an arbitrary waveform generator which RF output was directly modulated by the laser source. The output optical beam was

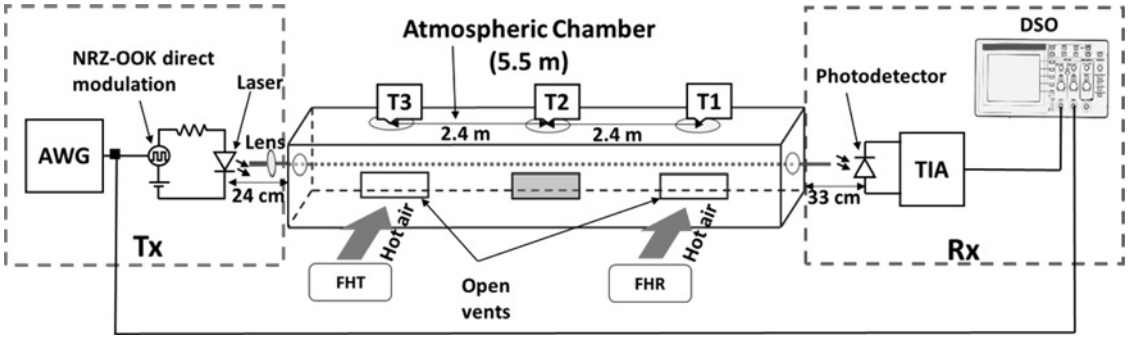

Fig. 1 *Schematic block diagram of the experimental set-up*

Table 1 Key system parameters

Parameters	Values
Tx	
data rate R_b	1, 5 and 10 Mbps
modulating signal V_{pp}	±200 mV
PSEUDO-random sequence of length	2^{16}–1 bits
optical source – laser	
wavelength λ	830 nm
optical output power P_{TX}	10 mW
bandwidth B_{TX}	75 MHz
Rx	
optical receiver – PIN PD	
active area A_{PD}	0.8 mm^2
bandwidth B_{RX}	150 MHz
responsivity R	0.35 A/W @ 830 nm
TIA	
transimpedance gain G_{TIA}	5–10 kΩ
butterworth filter bandwidth B_{BF}	1/2 data rate

collimated by a lens, positioned at 0.24 m from the laser diode output, prior to being launched into the chamber.

At the receiver side (Rx), a silicon PIN photodetector with an integrated trans-impedance amplifier (TIA) – to better detect the output photocurrent – was employed. The photodetector was positioned at 0.33 m from the chamber. Finally, the detected signal was captured by a high frequency digital storage oscilloscope (DSO) with a maximum analogue bandwidth of 2.5 GHz. At this stage both the transmitted and the recovered data (in NRZ-OOK formats) were captured by DSO for post-detection signal processing.

The key system parameters are reported in Table 1.

3 Theoretical background for data analysis

The measured data were post-processed to analyse the FSO link performance and to compare the results with the theoretical prediction. The received signal can be described by the conventional channel model [29]

$$y_k = hRx_k + n_o \tag{1}$$

where the channel state $h = h_t h_a$ where h_t and h_g are the attenuations because of the atmospheric turbulence, and geometric spread and pointing errors, respectively. $x_\kappa \in \{0, 2P_{Tx}\}$ is the optical intensity of the transmitted signal with P_{Tx} being the average transmitted optical power, R the responsivity of the photodetector at the optical transmission wavelength, and n_o is signal-independent additive white Gaussian noise with zero mean and variance σ_n^2. For a slow-fading channel with OOK signalling, the received electrical signal-to-noise ratio (SNR) is defined as [1]

$$\mathrm{SNR}(h)_{\mathrm{OOK}} = \frac{2P_{Tx}^2 R^2 h^2}{\sigma_n^2} \tag{2}$$

where SNR is a fluctuating term because of the influence of h, which is chosen from the random ensemble according to the distribution $f_h(h)$.

The signal received from the detector was digitally filtered via a second-order Butterworth low-pass filter with a cut-off frequency equal to half of the data rate. Since during the measurements we used oversampling to ensure high resolution, for data post-processing a down-sampling was adopted by selecting the points that maximise the Q-factor (and dually minimise the bit error rate [BER]). The BER defined in terms of the Q-factor can be expressed by [1, 30]

$$\mathrm{BER} = \frac{1}{2}\mathrm{erfc}\left(\frac{Q}{\sqrt{2}}\right) \tag{3}$$

where the Q-factor is

$$Q = \frac{v_H - v_L}{\sigma_H + \sigma_L} \tag{4}$$

v_H and v_L are the mean received voltages and σ_H and σ_L are the standard deviations for the 'high' and 'low' level signals, respectively.

Following the selection of the samples that maximise the Q-factor, the comparison with the theoretically predicted distributions was performed. In fact, as already explained in Section 1, several models are reported in literature to estimate optical turbulence effects. Since the aim of the experimental campaign was to assess the link performance under the weak turbulence condition, which is far more easier to generate, we chosen the G–G model – that can be used from weak-to-strong turbulence regimes – in order to compare the measured data with the predicted ones. The scintillation index presents a viable statistical quantitative measure of the magnitude of atmospheric turbulence-induced irradiance fluctuations (i.e. the level of scintillations) given by [11, 12]

$$\sigma_I^2 = \frac{\langle I^2 \rangle}{\langle I \rangle^2} - 1 \tag{5}$$

where the quantity I indicates the irradiance of the optical wave and the angle brackets $\langle . \rangle$ denote an ensemble average equivalent to long-time averaging with the assumption of an ergodic process. The classification of atmospheric turbulence-induced scintillations (i.e. weak, moderate and strong turbulences) is commonly distinguished through the values of the Rytov variance

$$\sigma_R^2 = 1.23 C_n^2 k^{7/6} L^{11/6} \tag{6}$$

where $k = 2\pi/\lambda$ is the optical wave number with λ being the laser wavelength and L is the distance from the transmitter. The refractive index structure parameter C_n^2 (in unit of $m^{-2/3}$) is physically interpreted as a measure of the strength of the fluctuations in the index of refraction, and is expressed through the relation [1]

$$C_n^2 = \left(79 \times 10^{-6} \frac{P}{T^2}\right)^2 C_T^2 \tag{7}$$

where C_T^2 denotes the temperature structure constant. The typical values of C_n^2 are $10^{-17}\,m^{-2/3}$ and $10^{-13}\,m^{-2/3}$ for weak and strong turbulence regimes, respectively. $\sigma_R^2 < 1$, $\sigma_R^2 \sim 1$ and $\sigma_R^2 \gg 1$ correspond to the weak, moderate and strong turbulence regimes, respectively.

According to the G–G model, the PDF of the received optical irradiance can be expressed as

$$p(I) = \frac{2(\alpha\beta)^{(\alpha+\beta)/2}}{\Gamma(\alpha)\Gamma(\beta)} I^{\{[(\alpha+\beta)/2]-1\}} K_{\alpha-\beta}\left(2\sqrt{\alpha\beta I}\right) \tag{8}$$

where $\Gamma(\cdot)$ is the Gamma function, $K_n(\cdot)$ is the modified Bessel function of the second kind of order n, whereas α

doi: 10.1049/iet-com.2014.0432

and β are two parameters related to the large-scale and small-scale scintillations of the optical wave expressed, for plane wave model at zero inner scale case [12], as follows

$$\alpha = \left\{ \exp\left[\frac{0.49\sigma_R^2}{\left(1 + 1.11\sigma_R^{12/5}\right)^{7/6}} \right] - 1 \right\}^{-1} \tag{9}$$

$$\beta = \left\{ \exp\left[\frac{0.51\sigma_R^2}{\left(1 + 0.69\sigma_R^{12/5}\right)^{5/6}} \right] - 1 \right\}^{-1} \tag{10}$$

For a point detector and under weak turbulence conditions ($\sigma_R^2 << 1$) the scintillation index corresponds to the Rytov variance σ_R^2 that for the plane wave is defined as [11, 12]

$$\sigma_{I,pl}^2(0) = \sigma_R^2 = 1.23 C_n^2 k^{7/6} L^{11/6} \tag{11}$$

The aperture-averaging effect of a non-point receiver aperture is taken into account through the aperture-averaged scintillation index

$$\sigma_{I,pl}^2(D) = A_G \sigma_{I,pl}^2(0) \tag{12}$$

where A_G denotes the aperture-averaging factor and D is the receiver aperture diameter. The aperture-averaged scintillation index for the limiting plane-wave and spherical-wave models take on the forms

$$\sigma_{I,pl}^2(D) \cong \exp\left[\frac{0.49\sigma_R^2}{\left(1 + 0.65d^2 + 1.11\sigma_R^{12/5}\right)^{7/6}} + \frac{0.51\sigma_R^2\left(1 + 0.69\sigma_R^{12/5}\right)^{-5/6}}{1 + 0.90d^2 + 0.62d^2\sigma_R^{12/5}} \right] - 1 \tag{13}$$

where the scalar parameter d is given by

$$d = \sqrt{kD^2/4L} \tag{14}$$

The proposed channel model is capable of generating irradiance time series starting from the PDF given by (8), and to define a temporal correlation between the samples. The spatial relationship that links the optical irradiance values is given, in the case of a plane-wave propagation, by the following covariance function [11, 12] (see eqn. (15)) where ρ is the spatial variable, ${}_1F_1(\cdot)$ is the confluent hypergeometric function of first kind and η_x and η_y are two parameters, respectively, which are defined as [12, 27]

$$\eta_x = \frac{2.61}{1 + 1.11\sigma_R^{12/5}} \tag{16}$$

$$\eta_y = 3\left(1 + 0.69\sigma_R^{12/5}\right) \tag{17}$$

The above-mentioned spatial covariance is then converted into a time function by applying the Taylor's 'frozen eddies hypothesis' [11, 12, 27]. In detail, it is possible to define V_T as the average transverse wind speed (orthogonal to the propagation direction), and to express the spatial variable as a function of the time t

$$\rho = V_T t \tag{18}$$

Substituting (18) into (15), the covariance becomes a function of the only independent variable t, that is, $B_I(t)$.

A commonly-used method to simulate predictions of irradiance fluctuations is the theoretical block-fading model (BFM), where the channel fade remains constant during a block and then changes to another independent value in the following block [31]. By using this approach, it is not possible to obtain a time resolution that is less than one correlation time, that is, the time in which the amplitude of normalised covariance function is equal to 0.5 [25]. In order to improve the resolution, a time correlation between the irradiance samples has to be introduced. Our channel model uses an algorithm composed of a correlation filter and a non-linear memory-less block function [27]. The input parameters are the double side Fourier Transform of the temporal irradiance covariance $B_I(t)$ – and a random G–G irradiance time series. The temporal spacing between two adjacent samples is the reciprocal of the FFT sampling frequency f_c. Therefore it is possible to arbitrarily choose the temporal resolution of the sequence. This allows to achieve a higher accuracy than the above-mentioned BFM.

4 Measurement results

In this section the results of the measurement campaign carried out are discussed. For each data rate, as defined by Table 1, the performance of the FSO link with no turbulence was evaluated following the procedure outlined in Section 2. Table 2 summarises the measurement conditions and results obtained. As shown with no turbulence (i.e. cases 1, 4 and 6) the link quality is good judging by the values of the Q-factor – calculated using (4) – being > 20.

In Fig. 2*a*, we show the sampled signal (without the DC component) for the case 1 of Table 2. The black line represents the point-by-point average of the signal. As reported, the average irradiance is almost constant, thus indicating no or a very low turbulence within the chamber. In Fig. 2*b*, the corresponding eye-diagram is depicted, which is widely open, thus indicating very high link availability (i.e. low BER). In fact, the measured Q-factor is 47.6, whereas the BER – calculated using (3) – is almost zero.

$$B_I(\rho) = \exp\left[\left(\frac{0.49\sigma_R^2}{\left(1 + 1.11\sigma_R^{12/5}\right)^{7/6}} \right) {}_1F_1\left(\frac{7}{6}; 1; -\frac{k\rho^2\eta_x}{4L}\right) + \left(\frac{0.50\sigma_R^2}{\left(1 + 0.69\sigma_R^{12/5}\right)^{5/6}} \right) \left(\frac{k(\rho)^2\eta_y}{L}\right)^{5/12} K_{5/6}\left(\sqrt{\frac{k(\rho)^2\eta_y}{L}}\right) \right] - 1 \tag{15}$$

Table 2 Measurement conditions and results

Case	Data rate [Mbps]	T1 [°C]	T2 [°C]	T3 [°C]	Fan heater	*Q*-factor	BER	Scintillation index	Rytov variance
1	1	24	24	24	None	47.6	0	≃0	≃0
2	1	50	33	26	FHR	3.91	4.7×10^{-5}	0.004	0.006
3	1	24	25	35	FHT	1.81	3.5×10^{-2}	0.04	0.06
4	5	24	26	26	None	29.8	0	≃0	≃0
5	5	26	32	50	FHT	2.55	5.5×10^{-3}	0.01	0.013
6	10	25	27	26	None	21.2	0	0.0001	0.0002
7	10	36	29	25	FHR	3.22	6.5×10^{-4}	0.006	0.008
8	10	25	28	33	FHT	1.45	7.3×10^{-2}	0.07	0.096

Inducing turbulence through hot air inside the chamber the signal irradiance fluctuations were observed. In Fig. 3, the comparison between the sampled signal when the hot air fan was located at the receiver end for the case 7 (Fig. 3*a*), and at the transmitter end for the case 2 (Fig. 3*b*) is depicted. It is shown that greater irradiance fluctuations were recorded for case 2. This can be explained as follows. Within the chamber the optical beam is passing through the turbulence induced air bubbles of different sizes, experiencing scattering (phase fluctuation) and power loss [28]. In fact part of the scattered light beams are lost and the remaining propagates down the chamber to be collected at receiver. Thus the beam arriving at the receiver will have a much wider and fluctuated optical foot print, which is considerably larger than the area of the photodetector.

In Fig. 4*a*, the eye diagram corresponding to the case 2 is depicted. The eye opening is not as wide as in Fig. 2*a* because of turbulence within the chamber, thus indicating deterioration of the FSO link because of the low values of Q-factor (1.81) and the BER (3.53×10^{-2}). Fig. 4*b* shows the PDF of the measured samples (in grey), which is being compared with predicted G–G PDF (in black) calculated – through (8) – taking into account the measured scintillation index (obtained by (5)).

The small discrepancy visible between the two PDF distributions is because of the small number of samples taken during the acquisition. Nevertheless, this is a good agreement between the predicted and measured distribution, thus confirming the effectiveness of the G–G model in weak turbulence conditions. Similar results were obtained for a number of different set of measurements.

As shown in Table 2, the maximum scintillation index that could be reached (case 8) is equal to 0.07, corresponding to a Rytov variance of 0.096. The latter has been calculated by inverting (13), taking into account the receiver diameter. In this case, the *Q*-factor is 1.45, which corresponds to a BER of 7.34×10^{-2}. Moreover, in all the measurements, the aperture averaging factor was calculated using (12), by taking into account the photodetector active area, being equal to 0.77.

5 Comparison with the theoretical time-correlated channel model

In the previous sections, the results of the measurements campaign that was carried out on an indoor FSO link were discussed. In particular, the analysis was focused on the FSO link performance metrics such as the *Q*-factor and the BER, and the turbulence strength in terms of the scintillation index and Rytov variance. In addition, in order to investigate the temporal and frequency characteristics of the irradiance fluctuations, additional analysis on the collected data was also performed.

In detail, this section outlines the results obtained by using an irradiance time-series generator based on the channel model already reported in our previous works [27] and described in Section 3. In each experimental case, the temporal covariance of the signal was derived to obtain information on the frequency spectrum of the irradiance fluctuations. The measured scintillation index value was used to generate the samples with correct statistical distributions in accordance to the experimental turbulence condition. The theoretical temporal covariance $B_I(t)$ [27] – obtained by combining (15) and (18) – was then employed to temporally correlate the samples. Starting from the data collected during the measurements, the correct transverse wind speed value V_T (see (18)) was also determined, for each case, as a fitting parameter, in order to achieve a close matching between the measured and predicted temporal

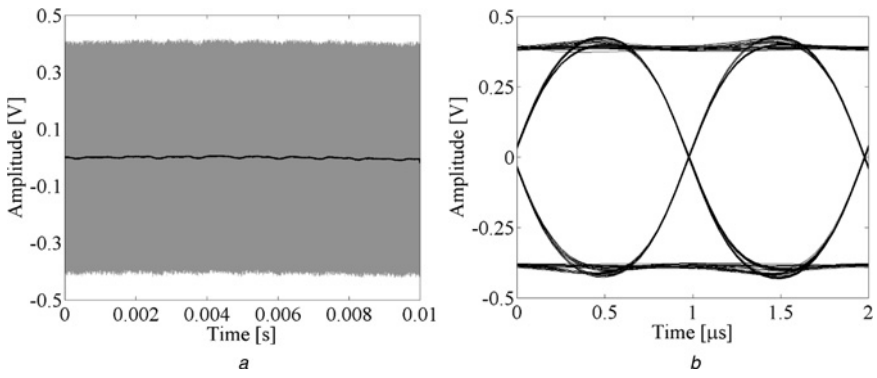

Fig. 2

a Sampled signal received at the photodetector (grey line) and the point-by-point average signal value (black line) for case 1
b Corresponding eye-diagram (plotted considering the first 4000 samples)

doi: 10.1049/iet-com.2014.0432

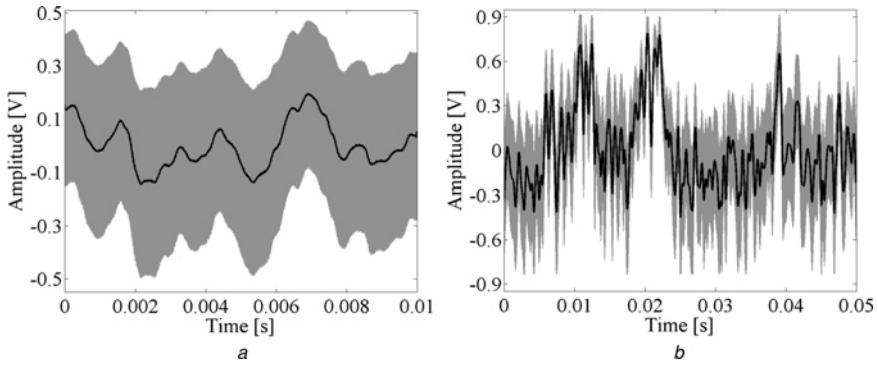

Fig. 3 *Sampled signal received by the photodetector (grey line) and the point-by-point average signal value (black line) in case 7 (a) and in case 2 (b)*

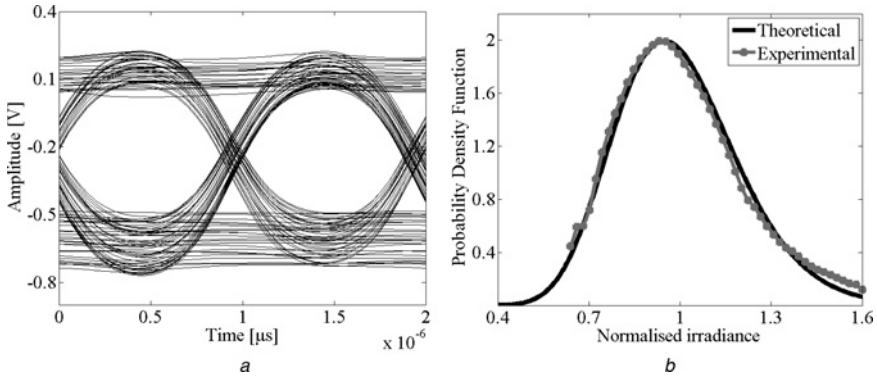

Fig. 4 *Case 2*

a Eye diagram
b PDF plots for measured samples and predicted using G–G distribution

covariances. The obtained values, summarised in Table 3, fall within the range of 0.4–2.6 m/s, comparable with the wind speeds measured by an anemometer placed nearby the vents, during the experimental campaign (about 1.5–2.5 m/s). Moreover, in Table 3 we show the comparison between the measured and predicted (from the theoretical temporal covariance) correlation times. Among all the above-mentioned cases, only those showing the presence of turbulence conditions are taken into account.

These values were used as input parameters for our channel model. Then, we have generated the irradiance time-series and compared them with the corresponding measured data in order to validate the model. We found that there is a close match between the time-series and measurement data distributions. Moreover, the temporal covariance of the time-series fits quite well – within a correlation time, reported in Table 3 – with the measured data. Fig. 5 shows both the PDF and normalised temporal covariance for the measured data and predicted time-series for the case 3 in Table 2.

In addition, a complete analysis tool was implemented in order to perform an in-depth simulation of the above-described experimental FSO link. In detail, it is composed of an FSO link simulator – that makes use of the equations illustrated in Section 3 – and also of the above-mentioned irradiance time-series generator. The tool is able to reproduce the employed experimental FSO link taking into consideration turbulence effects and noise contributions. Moreover, it can also evaluate the link performance by means of determining the Q-factor and BER.

In the simulations, all the parameters were set in accordance with the FSO link specifications. In particular, for each case, the average power intensity of the simulated NRZ OOK optical signal was set to the experimental value measured with no turbulence. In order to correctly reproduce the experimental conditions, a term of noise with the measured standard deviation of $\sim$70 mV was added to the simulated output signal of the photodetector. The obtained results are summarised in Table 4 and highlight a good agreement between measured and simulated data.

Table 3 Transverse wind speed and correlation times

Case	Data rate [Mbps]	Rytov variance	Transverse wind speed [m/s]	Measured correlation time [ms]	Predicted correlation time [ms]
2	1	0.006	2.0	0.35	0.34
3	1	0.06	1.5	0.44	0.45
5	5	0.013	2.4	0.30	0.29
7	10	0.008	1.7	0.41	0.42
8	10	0.096	0.7	0.94	0.94

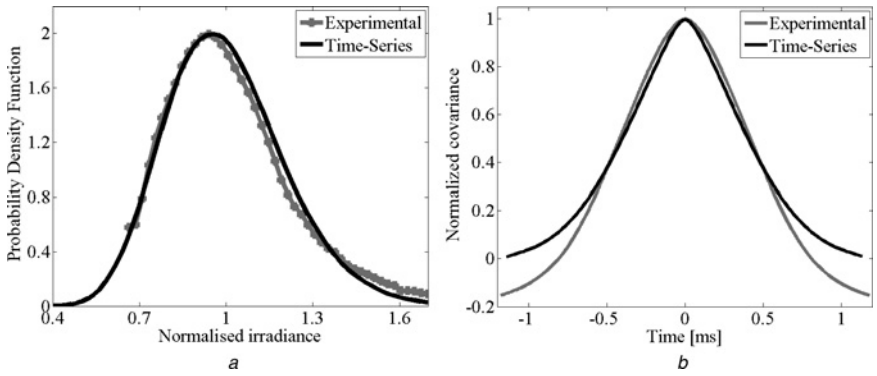

Fig. 5 *Comparison between the measured data and predicted time-series for*

a PDF

b Normalised temporal covariance for the case 3

Table 4 Comparison between measured and simulated Q-factors

Case	Data rate [Mbps]	Scintillation index	Measured Q-factor	Minimum simulated Q-factor	Mean simulated Q-factor	Maximum simulated Q-factor
2	1	0.004	3.91	3.09	4.51	6.71
3	1	0.04	1.81	1.29	1.65	2.33
5	5	0.01	2.55	2.15	3.13	4.71
7	10	0.006	3.22	2.51	3.91	6.08
8	10	0.07	1.45	1.22	1.47	1.91

Note that in all cases (with a notable level of turbulence) the measured Q-factor value falls well within the statistical distribution obtained by means of simulations.

For example, in Figs. 6*a* and *b* we show the simulated statistical distribution for the Q-factor (in black), which is compared with the measured value for the case 3 and 8, respectively, which present, among all the performed measurements, the higher turbulence condition generated within the atmospheric chamber.

The overall results are summarised in Fig. 7, which depicts the Q-factor against the scintillation index for the measured and the simulated maximum, mean, minimum values. As shown, for all cases the Q-factor decreases with increasing scintillation index and, furthermore, all the measured values fall within the range of the simulation results.

The close agreement between simulation and measured results highlights that the time-series generator is able to predict, with good approximation, the signal fluctuations and, consequently, enables the evaluation of the performance of a generic FSO link under the weak turbulence regime. This kind of approach can be useful for parametric studies of FSO link design, Monte Carlo analysis and, in addition, to study the performance of fading mitigation techniques. In detail, it is possible to automatically evaluate – in a more realistic way – the FSO link performance by establishing the exact time interval in which fading events can occur during communication, for the given turbulence condition and FSO link specifications. In this way, the packet loss (and hence the packet error rate – PER) occurring for a given situation can be evaluated, and it is also possible to obtain each single bit affected by the fading event.

Starting from the above-described FSO link and from the turbulence conditions reached in the chamber, some additional simulations were performed, to demonstrate the usefulness of our channel model for an FSO system designer. In detail, these simulations were aimed to obtain

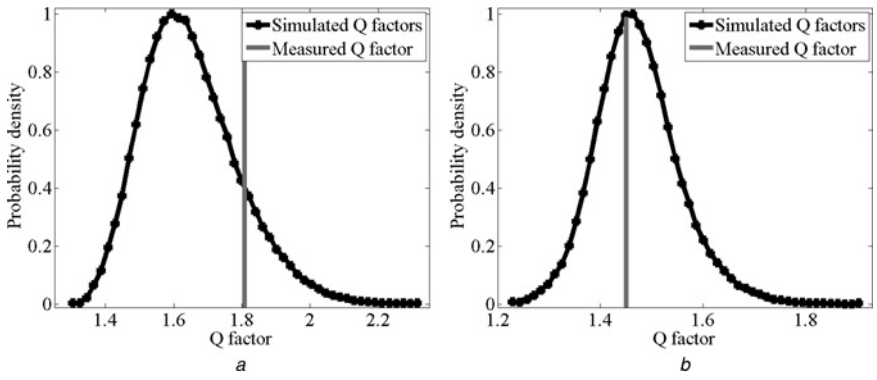

Fig. 6 *Simulated and measured probability density against the Q-factor values for*

a Case 3

b Case 8

doi: 10.1049/iet-com.2014.0432

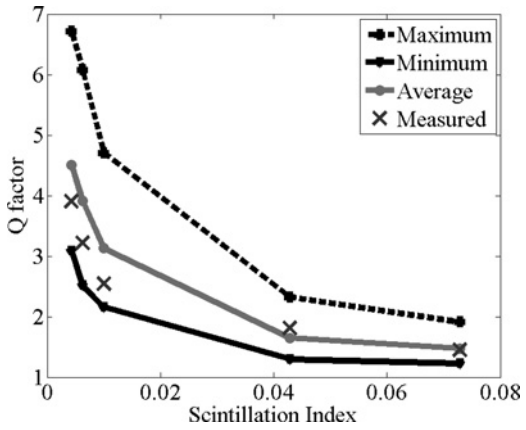

Fig. 7 *Q factor against scintillation index for the measured and the simulated maximum, mean, minimum values*

the PER, at varying FSO link path length and receiver active area. The worst turbulence condition obtained in the chamber (case 8), that is, Rytov variance of 0.096, was assumed as the test environment for the simulations. The other parameters were: fading depth threshold of 6 dB (i.e. the threshold, with respect to the average optical power, below which a packet is considered lost), packet length equal to 1000 bytes and 1 000 000 packets sent for each run. To obtain a higher accuracy, 20 cycles of simulations were performed for each combination of path length and receiver diameter. The results, in terms of PER, are shown in Fig. 8.

As reported, at increasing path length, the number of lost packets increases and hence the PER. Instead, at increasing receiver active area, it is possible to reduce packet loss and PER (because of the aperture averaging effect).

Finally, an additional simulation analysis was performed, this time at varying turbulence conditions and receiver area. In particular, the simulated configuration used the following parameters: the path length of the employed FSO set-up, a data rate of 10 Mbps and a transverse wind speed value of 0.7 m/s, whereas the Rytov variance was varied from 0.05 up to 0.4. Moreover, three different receiver active areas were considered ($A_{PD} = 0.08$ mm^2, $A_{PD} = 0.8$ mm^2 and $A_{PD} = 8$ mm^2). The results are summarised in Table 5.

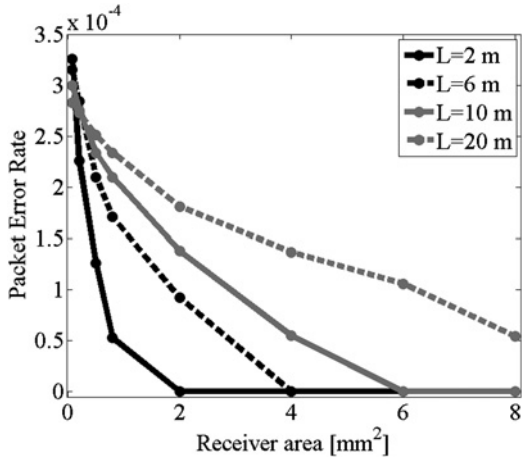

Fig. 8 *PER against receiver active area, at different path lengths and at Rytov variance = 0.096*

Table 5 PER at several combinations of Rytov variance and receiver active area

Rytov variance	PER		
	$A_{PD} = 0.08$ mm^2	$A_{PD} = 0.8$ mm^2	$A_{PD} = 8$ mm^2
0.05	0	0	0
0.1	4.04×10^{-4}	2.07×10^{-4}	0
0.15	4.09×10^{-3}	1.95×10^{-3}	4.37×10^{-5}
0.20	1.48×10^{-2}	8.14×10^{-3}	2.16×10^{-4}
0.25	3.25×10^{-2}	1.96×10^{-2}	6.80×10^{-4}
0.30	5.54×10^{-2}	3.56×10^{-2}	1.84×10^{-3}
0.35	8.16×10^{-2}	5.47×10^{-2}	3.91×10^{-3}
0.4	1.09×10^{-1}	7.57×10^{-2}	6.93×10^{-3}

As reported, the PER strongly increases with Rytov variance at a given active area. Instead, at a given turbulence condition, as expected, the PER strongly decreases when increasing the receiver active area. Therefore we can conclude that our channel model and the implemented simulator represent a very useful tool, that can be easily employed by system designers to choose the FSO link specifications suitable to have, for example, a maximum PER or BER.

6 Conclusions

In this paper, an indoor FSO link performance was assessed using an indoor laboratory atmospheric chamber where turbulence conditions were created. The obtained results showed that turbulence can severely affect the link performance, decreasing the Q-factor and increasing the BER, even under weak turbulence conditions. A maximum value for Rytov variance of 0.096 (measuring a BER of 7.3×10^{-2}) was obtained. Moreover, a complete analysis tool able to perform an in-depth simulation of the experimental FSO links was implemented. In this way, we were able to test, for the first time, our time-correlated channel model, which can be used to generate time-series to predict the irradiance fluctuations – caused by optical turbulence – observed at the receiver. The generated time-series were compared with the experimental data collected during the measurement campaign, showing a good agreement and thus proving the effectiveness of the model. Hence, we can conclude that, by properly setting the simulation parameters, it is possible to employ the proposed model to evaluate with good approximation – by using a simulation approach – the performance of a FSO link under several turbulence conditions, in terms of Q-factor, BER, PER and errors caused by fading. In the near future, we aim to examine the validity of the model also under moderate-to-strong turbulence conditions, for example by generating higher temperature gradients within the chamber.

7 Acknowledgments

This work was supported by the European Space Agency under grant no. 5401001020. We are very grateful to Dr. E. Armandillo for enlightening discussions. J. Perez's work was support by Spanish MINECO Juan de la Cierva Fellowship JCI-2012-14805. This research project falls within the frame of COST ICT Action IC1101 – Optical Wireless Communications – An Emerging Technology (OPTICWISE).

8 References

1 Ghassemlooy, Z., Popoola, W., Rajbhandari, S.: 'Optical wireless communications: system and channel modelling with MATLAB' (CRC Press, Boca Raton, FL, 2012)
2 Tsukamoto, K., Hashimoto, A., Aburakawa, Y., Matsumoto, M.: 'The case for free space', *IEEE Microw. Mag.*, 2009, **10**, (5), pp. 84–92
3 Majumdar, A.K., Ricklin, J.C.: 'Free-space laser communications: principles and advances' (Springer, New York, 2008)
4 Leitgeb, E., Awan, M.S., Plank, T., *et al.*: 'Investigations on free-space optical links within SatNEx II'. Proc. Third European Conf. on Antennas and Propagation (EuCAP 2009), Berlin, Germany, 23–27 March 2009, pp. 1707–1711
5 Naimullah, B.S., Othman, M., Rahman, A.K., *et al.*: 'Comparison of wavelength propagation for free space optical communications'. Proc. 2008 IEEE Int. Conf. on Electronic Design (ICED 2008), Penang, Malaysia, 1–3 December 2008, pp. 1–5
6 Report ITU-R F.2106-1: 'Fixed service applications using free-space optical links'. 2010
7 Suriza, A.Z., Md Rafiqul, I., Wajdi, A.K., Naji, A.W.: 'Proposed parameters of specific rain attenuation prediction for free space optics link operating in tropical region', *J. Atmos. Sol-Terr. Phy.*, 2013, **94**, pp. 93–99
8 Fiser, O., Schejbal, V.: 'Comparison of formulas estimating fog attenuation on free space optics links'. Proc. Fourth European Conf. on Antennas and Propagation (EuCAP 2010), Barcelona, Spain, 12–16 April 2010, pp. 1–4
9 Nebuloni, R.: 'Empirical relationships between extinction coefficient and visibility in fog', *Appl. Opt.*, 2005, **44**, (18), pp. 3795–3804
10 Mori, S., Marzano, F.S., Frezza, F., *et al.*: 'Model analysis of hydrometeor scattering effects on free space near-infrared links'. Proc. Int. Workshop on Optical Wireless Communications (IWOW 2012), Pisa, Italy, 22 October 2012, pp. 1–3
11 Andrews, L.C., Phillips, R.L., Hopen, C.Y.: 'Laser beam propagation through random media' (SPIE Press, Bellingham, WA, 2005, 2nd edn.)
12 Andrews, L.C., Phillips, R.L., Hopen, C.Y.: 'Laser beam scintillation with applications' (SPIE Press, Bellingham, WA, 2001)
13 Khalighi, M.-A., Aitamer, N., Schwartz, N., Bourennane, S.: 'Turbulence mitigation by aperture averaging in wireless optical systems'. Proc. 10th Int. Conf. on Telecommunications (ConTEL 2009), Zagreb, Croatia, 8–10 June 2009, pp. 59–66
14 Malpani, A., Malpani, A.: 'Performance analysis of FSO communication with aperture averaging under varying atmospheric turbulence Regimes'. Proc. Ninth Int. Conf. on Wireless and Optical Communications Networks (WOCN 2012), Indore, India, 20–22 September 2012, pp. 1–6
15 Weerackody, V., Hammons, A.R., Tebben, D.J.: 'Multi-input multi-output free space optical satellite communication links'. Proc. 41st Annual Conf. on Information Sciences and Systems (CISS '07), Baltimore, MD, USA, 14–16 March 2007, pp. 679–683
16 García-Zambrana, A., Castillo-Vázquez, C., Castillo-Vázquez, B.: 'Outage performance of MIMO FSO links over strong turbulence and misalignment fading channels', *Opt. Express*, 2011, **19**, (14), pp. 13480–13496
17 Luby, M.: 'LT codes'. Proc. 43rd Annual IEEE Symp. on Foundations of Computer Science, Vancouver, Canada, 16–19 November 2002, pp. 271–280
18 Shokrollahi, A.: 'Raptor codes', *IEEE Trans. Inf. Theory*, 2006, **52**, (6), pp. 2551–2567
19 MacKay, D.J.C.: 'Fountain codes', *IEE P-Commun.*, 2005, **152**, (6), pp. 1062–1068
20 Uysal, M., Jing, L., Meng, Y.: 'Error rate performance analysis of coded free-space optical links over gamma-gamma atmospheric turbulence channels', *IEEE Trans. Wirel. Commun.*, 2006, **5**, (6), pp. 1229–1233
21 Tsiftsis, T.A.: 'Performance of heterodyne wireless optical communication systems over gamma-gamma atmospheric turbulence channels', *Electron. Lett.*, 2008, **44**, (5), pp. 372–373
22 Popoola, W.O., Ghassemlooy, Z.: 'BPSK subcarrier intensity modulated Free-Space Optical Communications in atmospheric turbulence', *J. Lightwave Technol.*, 2009, **27**, (8), pp. 967–973
23 Nistazakis, H.E., Tsiftsis, T.A., Tombras, G.S.: 'Performance analysis of free-space optical communication systems over atmospheric turbulence channels', *IET Commun.*, 2009, **3**, (8), pp. 1402–1409
24 Bayaki, E., Schober, R., Mallik, R.K.: 'Performance analysis of MIMO free-space optical systems in gamma-gamma fading', *IEEE Trans. Commun.*, 2009, **57**, (11), pp. 3415–3424
25 Anguita, J.A., Neifeld, M.A., Hildner, B.: 'Rateless coding on experimental temporally correlated FSO channels', *IEEE J. Lightwave Technol.*, 2010, **28**, (7), pp. 990–1002
26 Anguita, J.A., Cisternas, J.E.: 'Turbulence strength and temporal correlation in a terrestrial laser communication link'. Proc. SPIE 7814, Free-Space Laser Communications X, 78140H, 2010
27 Andò, A., Mangione, S., Curcio, L., Stivala, S., Garbo, G., Pernice, R., Busacca, A.C.: 'Recovery capabilities of rateless codes on simulated turbulent terrestrial free space optics channel model', *Int. J. Antennas Propag.*, 2013, **2013**, Article ID 692915, p. 8
28 Ghassemlooy, Z., Le Minh, H., Rajbhandari, S., Perez, J., Ijaz, M.: 'Performance analysis of Ethernet/fast-Ethernet free space optical communications in a controlled weak turbulence condition', *J. Lightwave Technol.*, 2012, **30**, (13), pp. 2188–2194
29 Zhu, X.M., Kahn, J.M.: 'Free-space optical communication through atmospheric turbulence channels', *IEEE Trans. Commun.*, 2002, **50**, (8), pp. 1293–1300
30 Agrawal, G.P.: 'Fiber-optic communications systems' (Wiley & Sons, New York, 2002, 3rd edn.)
31 Xu, F., Khalighi, A., Caussé, P., Bourennane, S.: 'Channel coding and time-diversity for optical wireless links', *Opt. Express*, 2009, **17**, (2), pp. 872–887

doi: 10.1049/iet-com.2014.0432